ADVANCED MATERIALS

Supporting Information

for *Adv. Mater.*, DOI: 10.1002/adma.201908424

Inverse Design Strategies for 3D Surfaces Formed by Mechanically Guided Assembly

Zhichao Fan, Yiyuan Yang, Fan Zhang, Zheng Xu, Hangbo Zhao, Taoyi Wang, Honglie Song, Yonggang Huang, John A. Rogers,* and Yihui Zhang**

Supporting Information

Inverse design strategies for 3D surfaces formed by mechanically guided assembly

Zhichao Fan†, Yiyuan Yang†, Fan Zhang, Zheng Xu, Hangbo Zhao, Taoyi Wang, Honglie Song, Yonggang Huang, John A. Rogers*, and Yihui Zhang**

[*] Prof. Yihui Zhang, Corresponding-Author
Applied Mechanics Laboratory, Department of Engineering Mechanics; Center for Flexible Electronics Technology
Tsinghua University
Beijing 100084 (P.R. China)
E-mail: yihuizhang@tsinghua.edu.cn

[*] Prof. John A. Rogers, Corresponding-Author
Department of Materials Science and Engineering, Biomedical Engineering, Neurological Surgery, Chemistry, Mechanical Engineering, Electrical Engineering and Computer Science
Simpson Querrey Institute and Feinberg Medical School
Center for Bio-Integrated Electronics
Northwestern University
Evanston, Illinois 60208 (USA)
E-mail: jrogers@northwestern.edu

[*] Prof. Yonggang Huang, Corresponding-Author
Departments of Civil and Environmental Engineering, Mechanical Engineering, and Materials Science and Engineering, Center for Bio-Integrated Electronics Northwestern University
Evanston, IL 60208 (USA)
E-mail: y-huang@northwestern.edu

Dr. Zhichao Fan, Dr. Fan Zhang, Mr, Zheng Xu, Dr. Honglie Song
Applied Mechanics Laboratory, Department of Engineering Mechanics; Center for Flexible Electronics Technology
Tsinghua University
Beijing 100084 (P.R. China)

Mr. Yiyuan Yang
Departments of Mechanical Engineering
Northwestern University
Evanston, Illinois 60208 (USA)

Mr. Zheng Xu
The State Key Laboratory for Manufacturing and Systems Engineering, School of Mechanical Engineering

Xi'an Jiaotong University
Xi'an 710049 (P.R. China)

Dr. Hangbo Zhao
Center for Bio-Integrated Electronics
Northwestern University
Evanston, Illinois 60208 (USA)

Mr. Taoyi Wang
Department of Physics
Tsinghua University
Beijing 100084 (P.R. China)

†These authors contributed equally to this work.

Keywords: 3D assembly, 3D mesostructures, Inverse design, Analytic modeling

Contents

S1 Inverse design of curvy ribbons

S1.1 Inverse design of simply-supported ribbons

S1.2 Inverse design of combined ribbons

S1.3 Examples

S2 Inverse design of centrally symmetric 3D surfaces

S2.1 Inverse design approach

S2.2 Examples

S3 Inverse design of general 3D surfaces

S3.1 Inverse design approach

S3.2 Examples

S4 Cartoon face

S1 Inverse design of curvy ribbons

This section presents the theoretical analysis on two types of curvy ribbons, including the simply-supported ribbons and combined ribbons that consist of both the simply-supported ribbon and cantilever ribbons. The internal moment and bending curvature of these ribbons resulted from a given load can be determined directly from the static equilibrium equations. As such, it is possible to obtain inverse design solutions in an explicit analytical form. Details of the inverse design of the structures illustrated in Fig.1 are given in the end of this section.

S1.1 Inverse design of simply-supported ribbons

Consider a straight ribbon of length L_S with creases in two ends. The forces due to the release of a pre-stretched substrate transform the straight ribbon into the curvy ribbon via out-of-plane bending, as illustrated in Fig. S1a. The bending deformations occur mostly at creases with small thicknesses, because the bending stiffness is proportional to the cube of the thickness. Thus, we model the ribbon as a simply-supported beam subjected to uniaxial compressive force P, as illustrated in the Fig. S1b. Furthermore, the thin, narrow geometry of the ribbon allows us to neglect the axial elongation in following analysis. The applied strain ε_{app} of the ribbon and the pre-strain ε_{pre} of the substrate are defined as

$$\varepsilon_{\text{app}} = \frac{L_S - L}{L_S}, \tag{S1}$$

$$\varepsilon_{\text{pre}} = \frac{L_S - L}{L + L_{\text{bonding}}}, \tag{S2}$$

where $L = X(L_S) - X(0)$ is the distance between two ends in the deformed configuration. The static equilibrium of the curvy ribbon requires

$$m(S) = E(S)I(S)K(S) = E(S)\frac{w(S)[t(S)]^3}{12}K(S) = PZ(S), \tag{S3}$$

where $m(S)$, $E(S)$ and $I(S)$ are the moment, Young's modulus, and the moment of inertia, respectively. As for a given axis shape ($X(S)$ and $Z(S)$) of the curvy ribbon, the thickness distribution can be derived from the above equation, i.e.,

$$t(S) = \left[\frac{12PZ(S)}{E(S)K(S)w(S)}\right]^{\frac{1}{3}}. \tag{S4}$$

Then the load P can be written as

$$P = \frac{t_{\max}^3}{\max\left[\frac{12Z(S)}{E(S)K(S)w(S)}\right]}, \tag{S5}$$

in which $t_{\max}$ is the maximum thickness value used in the experiment. Substitution of Eq. (S5) into Eq. (S4) gives

$$t(S) = \frac{t_{\max}\left[\frac{Z(S)}{E(S)w(S)K(S)}\right]^{\frac{1}{3}}}{\max\left[\frac{Z(S)}{E(S)w(S)K(S)}\right]^{\frac{1}{3}}}, \tag{S6}$$

in which the Young's modulus $E(S)$ is usually set as a constant value in the experiment. Consequently, the thickness distribution $t(S)$ can be fully determined by the geometrical information of the target 2D ribbons.

Next, we focus on restrictions of the axis shape of the target 2D ribbons. The ends of the structure are bonded on the substrate (referred to as bonding sites), and the ribbon cannot penetrate the substrate during the buckling process. The coordinate value $Z(S)$ of the target ribbon satisfy

$$\begin{aligned} &Z(0)=Z(L_S)=0 \\ &Z(S)>0, S\in(0,L_S) \end{aligned}. \tag{S7}$$

Using Eq. (S3), the curvature $K(S)$ of the axis shape also needs to be positive along the arc length, i.e.,

$$K(S)=\frac{PZ(S)}{E(S)I(S)}>0, S\in(0, L_S). \tag{S8}$$

The thickness distribution of the 2D precursor is determined by Eq. (S6) when the axis shape of the target 2D ribbon meets the above conditions (Eqs. (S7) and (S8)). To this end, we obtain all geometrical parameters, including the given width $w(S)$, the arc length L_S, the bonding length L_{bonding} and the thickness distribution $t(S)$.

Next, when the target structure's axis curvature is not positive everywhere, additional forces need to be applied to the ribbon to meet the conditions for static equilibrium. In Fig. S2a, we demonstrate a simply-supported ribbon model subjected to the uniaxial compressive force P at ends and several vertical

concentrated forces $G_i\left(i=1,2,\cdots n\right)$ at the points $S_i\left(i=1,2,\cdots n\right)$. The static equilibrium gives the reaction force G_0 and G_{n+1} as

$$\begin{aligned} G_0 &= \frac{1}{X\left(L_S\right)}\sum_{i=1}^{i=n} G_i X\left(S_i\right) - \sum_{i=1}^{i=n} G_i \\ G_{n+1} &= -\frac{1}{X\left(L_S\right)}\sum_{i=1}^{i=n} G_i X\left(S_i\right). \end{aligned} \quad . \tag{S9}$$

Then the piecewise static equilibrium of the ribbon model gives

$$\sum_{j=i+1}^{j=n+1} G_j\left[X\left(S_j\right)-X\left(S\right)\right]+PZ\left(S\right)=E\left(S\right)I\left(S\right)K\left(S\right),\ S\in\left[S_i,S_{i+1}\right],\ \left(i=0,1,2,\cdots,n\right), \tag{S10}$$

in which $S_0=0$, $S_{n+1}=L_S$. When no concentrated force G_i is loaded on the ribbon, the above equilibrium equation can then be simplified to Eq. (S3). In other words, we can design the curvy ribbon inversely with more general shape by applying concentrated forces G_i to the ribbon. As for a given axis shape ($X(S)$, $Z(S)$ and $K(S)$), the number n has a lower limit. To avoid multiple solutions from the inverse design, the symbol n refers to the smallest number of forces G_i that the static equilibrium (Eqs. (S10)) requires in the following analysis. Assume that the target curvature $K(S)$ has k zero points $S_{K(i)},\left(i=1,2,\cdots k\right)$, namely $K\left(S_{K(i)}\right)=0$. By making a preliminary estimate on the relative position between $S_{K(i)}$ and S_i, Eqs. (S10) gives

$$\sum_{j=l+1}^{j=n+1} G_j\left[X\left(S_j\right)-X\left(S_{K(i)}\right)\right]+PZ\left(S_{K(i)}\right)=0,\ S_{K(i)}\in\left[S_l,S_{l+1}\right],\ \left(i=1,2,\cdots,k\right). \tag{S11}$$

The above independent equations are used to obtain the magnitudes of the forces G_i and the loading positions S_i. The equality between the number of equations and the number of unknowns requires

$$n = k/2 . \tag{S12}$$

The loading position S_i obtained from Eqs. (S11) should be utilized to verify the preliminary estimate $S_{K(i)} \in [S_l, S_{l+1}]$. A reasonable solution of the force magnitude G_i and the loading positions S_i can be inserted into Eqs. (S10) to give the final equilibrium equation of the target 2D ribbons. Similar to the ribbon with a positive curvature (Eqs. (S3)~(S6)), the thickness distribution $t(S)$ of the 2D precursor is obtained with the given maximum thickness $t_{\max}$. However, if there is no reasonable solution for G_i, the force number n should be increased. In this case, the number of unknowns exceeds the number of equations (Eqs. (S11)), and the solution of the force magnitudes G_i and the loading positions S_i is no longer unique. In other words, the thickness distribution $t(S)$ derived from Eqs. (S10) has multiple solutions.

As illustrated in Fig. S2b, we present a symmetric ribbon model that requires two vertical concentrated forces (G_1 and G_2) to satisfy the static equilibrium. Introduction of two inner ribbons of the 2D precursor in experiment (Fig. S2c) provides these concentrated forces. We take the inner ribbon on the left side, which provides the force G_1, as an example to present the design processes of the inner ribbon of the 2D precursor. We model the inner

ribbon as a cantilever beam with constant thickness t_{ribbon} and constant width w_{ribbon}. The bending stiffness is given by $EI_{\text{ribbon}} = Ew_{\text{ribbon}}t_{\text{ribbon}}^3/12$. The axis shape of the deformed ribbon is given by

$$z(x) = \frac{G_1}{6EI_{\text{ribbon}}}\left\{3\left[\frac{3EI_{\text{ribbon}}}{G_1}Z(S_1)\right]^{\frac{1}{3}} - x\right\}x^2,\ x \in \left[0, \left[\frac{3EI_{\text{ribbon}}}{G_1}Z(S_1)\right]^{\frac{1}{3}}\right]. \tag{S13}$$

Thus, the arc length of the inner ribbon is

$$L_{\text{ribbon}} = \int_0^{x_{\max}} \sqrt{1+\left(\frac{\mathrm{d}z}{\mathrm{d}x}\right)^2}\,\mathrm{d}x = \int_0^{\left[\frac{3EI_{\text{ribbon}}}{G_1}Z(S_1)\right]^{\frac{1}{3}}} \sqrt{1+\frac{G_1^2x^2\left\{2\left[\frac{3EI_{\text{ribbon}}}{G_1}Z(S_1)\right]^{\frac{1}{3}} - x\right\}^2}{4E^2I_{\text{ribbon}}^2}}\,\mathrm{d}x, \tag{S14}$$

and the length of the bonding site of the inner ribbon is

$$L_{\text{ribbon-bonding}} = \frac{1}{\varepsilon_{\text{pre}}}\left(L_S - 2S_1 + 2L_{\text{ribbon}}\right) - \frac{2+2\varepsilon_{\text{pre}}}{\varepsilon_{\text{pre}}}\left\{X\left(\frac{L_S}{2}\right) - X(S_1) + \left[\frac{3EI_{\text{ribbon}}}{G_1}Z(S_1)\right]^{\frac{1}{3}}\right\}. \tag{S15}$$

Because the inner ribbon is connected to the original large ribbon (e.g., 2D precursor in Fig. S2c), we set a small value of width w_{ribbon} (e.g., $\sim w/4$) in practice. Then, we obtain the reasonable values of arc length L_{ribbon} and bonding length $L_{\text{ribbon-bonding}}$ by setting a proper value of thickness t_{ribbon} in Eqs. (S14) and (S15). Moreover, since the end subjected to force is free to rotate in the cantilever beam model, we set a crease with thickness $t_{\text{ribbon}}/5$ in the inner ribbon end connecting to the large ribbon. The thickness $t(S)$ of the large ribbon section containing the inner ribbon and its bonding (e.g.,

$S \in \left[S_1 - L_{\text{ribbon}} - L_{\text{ribbon-bonding}}, S_1 \right] \cap \left[S_2, S_2 + L_{\text{ribbon}} + L_{\text{ribbon-bonding}} \right]$ in Fig. S2c) needs to be revised as $\left\{ w(S) / \left[w(S) - w_{\text{ribbon}} \right] \right\}^{\frac{1}{3}} t(S)$, as illustrated in Fig. 1b (D).

To this end, we obtain the design parameters of the 2D precursor, including the geometrical parameters and the pre-strain of the substrate, through the static equilibrium condition of the target curvy ribbon subjected to the forces induced by releasing the pre-stretched substrate.

In summary, for the target ribbon with positive curvature (Eq. (S8)), the axis shape is relatively simple, and the design (Eqs. (S2) and (S6)) obtained by static equilibrium is exactly the solution of the inverse design. For the target ribbon with several (k) zero points of axis curvature, which needs at least $k/2$ additional vertical forces to meet the equilibrium condition, then the solution of the inverse design is much more difficult to find.

S1.2 Inverse design of combined ribbons

This section focuses on the combined ribbon consisting of a cantilever ribbon and a simply-supported ribbon. As illustrated in Fig. S3a, the end of the cantilever ribbon is subjected to a concentrated force P with the loading angle θ. The moment equilibrium gives

$$m(S) = K(S) EI(S) = -P \left\{ \cos\theta \left[Z(L_S) - Z(S) \right] + \sin\theta \left[X(L_S) - X(S) \right] \right\}. \quad \text{(S16)}$$

Similar to the simply-supported ribbon, the magnitude of load P and the thickness distribution $t(S)$ are derived from the above equilibrium equation as

$$P=\frac{t_{\max}^{3}}{\max\left\langle\frac{-12\left\{\cos\theta\left[Z\left(L_S\right)-Z\left(S\right)\right]+\sin\theta\left[X\left(L_S\right)-X\left(S\right)\right]\right\}}{K\left(S\right)Ew\left(S\right)}\right\rangle} \tag{S17}$$

$$t\left(S\right)=\frac{t_{\max}\left\langle\frac{-\left\{\cos\theta\left[Z\left(L_S\right)-Z\left(S\right)\right]+\sin\theta\left[X\left(L_S\right)-X\left(S\right)\right]\right\}}{K\left(S\right)w\left(S\right)}\right\rangle^{\frac{1}{3}}}{\max\left\langle\frac{-\left\{\cos\theta\left[Z\left(L_S\right)-Z\left(S\right)\right]+\sin\theta\left[X\left(L_S\right)-X\left(S\right)\right]\right\}}{K\left(S\right)w\left(S\right)}\right\rangle^{\frac{1}{3}}}. \tag{S18}$$

So far, we complete the inverse design of the two parts (i.e., the simply-supported ribbon and the cantilever ribbon) of the combined ribbons. The Newton's third law defines the magnitude of the load P applied to the simply-supported ribbon to be the same as the load applied to the cantilever ribbon. The direction of the load coincides with the end-to-end line of the simply-supported ribbon, as illustrated in Fig. S3b. In the inverse design approach, we can set the maximum thickness value of the cantilever ribbon, then obtain the magnitude of load P using Eq. (S17), and then determine the maximum thickness value of the simply-supported ribbon using Eq. (S5). Hence, the thickness distributions (Eqs. (S6), (S18)) of these two parts are obtained with the given axis coordinates. The coordinate system used in Eqs. (S5) and (S18) is built for the simply-supported ribbon, as illustrated in Fig. S1b. In Fig. S3c, we illustrate the 3D assembly of the combined ribbon with two creases ($t\sim t_{\max}/16$) designed in the joint of two parts and the end on the right. These creases are also approximated as hinges in the model. In practice, we exploit the simply-supported part of the supporting ribbon in the combined structure, and set the cantilever part as the target shape.

Then, we focus on the reproduction of the target shape, namely the axis shape of the cantilever ribbon. Since the left end ($S=0$) of the cantilever ribbon is clamped (Fig. S3a), it requires

$$Z(0)=0,\left.\frac{\mathrm{d}Z(S)}{\mathrm{d}S}\right|_{S=0}=0. \tag{S19}$$

Furthermore, the use of Eq. (S16) and $\theta\in\left(0,\frac{\pi}{2}\right]$ gives

$$K(S)<0, S\in(0, L_S). \tag{S20}$$

Apart from the combined ribbon illustrated in Fig. S3, other combination forms of the cantilever ribbon (CR) and the simply-supported ribbon (SR), such as CR-SR-CR can be adopted in the 3D assembly. The mechanics analysis of these combinations is analogous to the above approach.

S1.3 Examples

Here, we present the axis coordinate information and the corresponding design parameters of the structures illustrated in Fig. 1b.

A (Circular arc)

The coordinates of the axis are

$$\begin{cases} X(S)=R\left[\sin\left(\frac{\alpha}{2}\right)-\sin\left(\frac{\alpha}{2}-\frac{S}{R}\right)\right] \\ Z(S)=R\left[\cos\left(\frac{\alpha}{2}-\frac{S}{R}\right)-\cos\left(\frac{\alpha}{2}\right)\right] \end{cases}, \ S\in[0, L_S], \tag{S21}$$

in which the arc length $L_S=100\,\mathrm{mm}$, the central angle $\alpha=2\pi/3$, and the radius $R=L_S/\alpha$. The width is set as w=5 mm. Using (S6) gives

$$t(S)=t_{\max}\left[\frac{\cos\left(\frac{\alpha}{2}-\frac{S}{R}\right)-\cos\left(\frac{\alpha}{2}\right)}{1-\cos\left(\frac{\alpha}{2}\right)}\right]^{1/3}, \tag{S22}$$

where the maximum thickness $t_{\max}=0.32\,\text{mm}$.

B (Asymmetrical shape)

$$\begin{cases} Z(S)=\dfrac{243(L_S-S)S\begin{pmatrix}158353L_S^4+43353L_S^3S+200853L_S^2S^2\\+211653L_SS^3-330237S^4\end{pmatrix}}{72500000L_S^5} \\ X(S)=\int_0^S\left[1-\left(\dfrac{\mathrm{d}Z(\xi)}{\mathrm{d}\xi}\right)^2\right]^{\frac{1}{2}}\mathrm{d}\xi \end{cases}, \; S\in[0,L_S], \tag{S23}$$

in which arc length $L_S=100\,\text{mm}$. The width is set as w=5 mm. Using (S6) gives

$$t(S)=\frac{t_{\max}}{\max\left[f(S)\right]^{\frac{1}{3}}}\left[f(S)\right]^{\frac{1}{3}}, \tag{S24}$$

where

$$f(S)=\frac{\left[\begin{array}{l}S(L_S-S)\begin{pmatrix}158353L_S^4+43353L_S^3S+200853L_S^2S^2\\+211653L_SS^3-330237S^4\end{pmatrix}\\ \times\sqrt{\begin{pmatrix}34020221L_S^5+55890000L_S^4S\\-114817500L_S^3S^2-10497600L_S^2S^3\\+658396350L_SS^4-481485546S^5\end{pmatrix}\begin{pmatrix}110979779L_S^5-55890000L_S^4S\\+114817500L_S^3S^2+10497600L_S^2S^3\\-658396350L_SS^4+481485546S^5\end{pmatrix}}\end{array}\right]}{\left(23000L_S^4-94500L_S^3S-12960L_S^2S^2+1083780L_SS^3-990711S^4\right)}.$$

C (Combined Shape)

The axis of the cantilever part is an arc with radius $R=30\,\text{mm}$ and the center angle $\alpha=\pi/2$. The loading angle is $\theta=\pi/5$. The axis of the simply-supported

part is an arc with radius $R = 120\,\text{mm}$ and center angle $\alpha = 2\,\text{arccsc}\left(2\sqrt{10-2\sqrt{5}}\right)$.

Then the axis coordinates of the combined ribbon can be written as

$$X(S) = \begin{cases} 30\sin\left(\dfrac{S}{30}\right), S \in [0, L_{S1}] \\ -18.275+120\cos\left(1.5495-\dfrac{S}{120}\right), S \in [L_{S1}, L_{S1}+L_{S2}] \end{cases}, \quad \text{(S25)}$$

$$Z(S) = \begin{cases} 30-30\cos\left(\dfrac{S}{30}\right), S \in [0, L_{S1}] \\ -79.861+120\sin\left(1.5495-\dfrac{S}{120}\right), S \in [L_{S1}, L_{S1}+L_{S2}] \end{cases}$$

in which $L_{S1} = 15\pi\,\text{mm}$ and $L_{S2} = 240\,\text{arc}\,\text{csc}\left(2\sqrt{10-2\sqrt{5}}\right)\text{mm}$ are the arc lengths of the cantilever part and the simply-supported part, respectively. The width of ribbon is $w = 5\,\text{mm}$. The maximum thickness of the cantilever part is set as $t_{\max} = 0.512\,\text{mm}$, and the thickness distribution of the 2D precursor can be obtained as

$$t(S) = \begin{cases} 0.28854\left[3.2361\cos\dfrac{S}{30} - 2.3511\left(\sin\dfrac{S}{30}-1\right)\right]^{1/3}, S \in [0, L_{S1}] \\ 0.23400\left[-117.26+120\cos\left(0.60700-\dfrac{S}{120}\right)\right]^{1/3}, S \in [L_{S1}, L_{S1}+L_{S2}] \end{cases}. \quad \text{(S26)}$$

The above thickness solution is zero at the joint ($S = L_{S1}$) and the right end ($S = L_{S1} + L_{S2}$). In the experiment and FEA, the small regions containing these two sections are set as creases with thickness $t = 0.032\,\text{mm}$.

D (Complex Shape)

$$\begin{cases} Z(S)=\dfrac{L_S}{120}\left[5-5\sqrt{5}+16\sin\left(\dfrac{4\pi S}{5L_S}+\dfrac{\pi}{10}\right)+4\cos\left(\dfrac{24\pi S}{5L_S}-\dfrac{2\pi}{5}\right)\right] \\ X(S)=\int_0^S\left[1-\left(\dfrac{\mathrm{d}Z(\xi)}{\mathrm{d}\xi}\right)^2\right]^{\frac{1}{2}}\mathrm{d}\xi \end{cases}, S\in[0,L_S], \quad \text{(S27)}$$

in which the arc length $L_S=150\,\mathrm{mm}$. The axis curvature has four zero points, and therefore, we need to apply at least two vertical concentrated forces to the ribbon. Due to the symmetry of the ribbon, we design two inner ribbons with the same geometrical parameters in the 2D precursor. The loading locations are obtained as $S_1=49.365\,\mathrm{mm}$ and $S_2=100.64\,\mathrm{mm}$. The arc length, the bonding length, the width and the thickness of the inner ribbon are L_{ribbon}=22.872 mm, $L_{\text{ribbon-bonding}}$=4.5 mm, $w_{\text{ribbon}}=2.5\,\mathrm{mm}$ and $t_{\text{ribbon}}=0.48\,\mathrm{mm}$ respectively. The bonding length, the width and the maximum thickness of the large ribbon are $L_{\text{bonding}}=10.876\,\mathrm{mm}$, $w=10\,\mathrm{mm}$ and $t_{\max}=0.32\,\mathrm{mm}$. The pre-strain of the substrate is $\varepsilon_{\text{pre}}=0.085379$. The profile of the thickness distribution of the large ribbon is shown in Fig. 1b (D).

E (Microscale experiment (Circular arc))

The axis coordinates is the same as Eq. (S21) with the following parameters: the arc length $L_S=10\,\mathrm{mm}$, the central angle $\alpha=2\pi/3$ and the radius $R=L_S/\theta$. The width of the ribbon is $w=1\,\mathrm{mm}$. The theoretical thickness distribution $t(S)$ is given by Eq. (S22), in which the maximum value is $t_{\max}=10\,\mu\mathrm{m}$. In microscale experiments, we discrete the continuous thickness distribution into n layers with thickness

$$t_i = t_{\max} - \frac{(i-1)(t_{\max} - t_{\min})}{n-1}, i = 1, 2, \cdots, n, \quad \text{(S28)}$$

in which $t_{\min} = t_{\max}/10$ is the thickness value of the creases. The arc coordinates of the ends of these layers are obtained by solving $t(S) = t_i$. The results of such approximation of the thickness for the microscale experiments are presented in Fig. 1b (E,F,G).

F (Microscale experiment (Asymmetrical shape))

The axis coordinates and the theoretical thickness distribution are the same as Eqs. (S23) and (S24), with the arc length $L_S = 10\,\text{mm}$. The width of the ribbon is $1\,\text{mm}$.

G (Microscale experiment (Combined Shape))

The axis shape of structure G is one tenth of the structure C.

H (Semicircles)

The arc lengths, the widths and the maximum thicknesses of these semicircles are $(L_S, w, t_{\max}) = (2, 0.2, 0.01)\,\text{mm}$, $(10, 1, 0.01)\,\text{mm}$ and $(50, 5, 0.32)\,\text{mm}$ for the microscale, millimeter scale and centimeter scale experiments, respectively. The thickness distribution of these structures are obtained by using Eq. (S22), with the central angle $\alpha = \pi$.

S2 Inverse design of centrally symmetric 3D surfaces

S2.1 Inverse design approach

Since the centrally-symmetric surfaces are mostly not developable and cannot be transformed directly from 2D precursors via compressive buckling, we approximate the surface with curvy ribbons and then utilize the solutions in **Sec. S1** to design the 2D precursor. As illustrated in Fig. S4a, the target surface is divided into n segments, and each segment is then reconstructed by a curvy ribbon whose axis shape is the same with the generatrix of the target surface. To quantitatively describe the error caused by such an approximation, we project the segment and the curvy ribbon onto the XY plane, and denote the maximum distance between the two edges as error δ, i.e.,

$$\delta = \max\left[\left(\sec\frac{\pi}{n}-1\right)X(S)\right], S\in[0,L_S]. \tag{S29}$$

Although error δ decreases with the number n for a given generatrix, the increase of n may significantly rise experimental difficulties. We set $n=10$ in the inverse design of the centrally symmetric surfaces shown in this paper. Here, we take the centrally symmetric surface with the generatrix illustrated in Fig. S4c as an example to present the inverse design approach. The resulting 2D precursor is illustrated in Fig. S4d. The target shape's generatrix curvature is positive everywhere (Eq. (S8)). The primary geometrical parameters of the 2D precursor are the width distribution $w(S)$ and the thickness distribution $t(S)$. The width distribution $w(S)$ is given by

$$w(S)=\frac{2\pi|X(S)|}{n}, S\in\left[0,\frac{L_S}{2}-aL_S\right]\cap\left[\frac{L_S}{2}+aL_S,L_S\right], \tag{S30}$$

in which $a \ll 0.5$, and the region $S \in \left(\frac{L_S}{2} - aL_S, \frac{L_S}{2} + aL_S \right)$ is the small undivided part connecting each ribbon part. The thickness of the small part is set as the thickness of the joint, and using (S6) gives

$$t(S) = \begin{cases} \dfrac{t_{\max} \left[\dfrac{Z\left(\frac{L_S}{2} - aL_S \right)}{K\left(\frac{L_S}{2} - aL_S \right) w\left(\frac{L_S}{2} - aL_S \right)} \right]^{\frac{1}{3}}}{\max \left[\dfrac{Z(S)}{K(S)w(S)} \right]^{\frac{1}{3}}}, S \in \left(\frac{L_S}{2} - aL_S, \frac{L_S}{2} + aL_S \right) \\ \dfrac{t_{\max} \left[\dfrac{Z(S)}{K(S)w(S)} \right]^{\frac{1}{3}}}{\max \left[\dfrac{Z(S)}{K(S)w(S)} \right]^{\frac{1}{3}}}, S \in \left[0, \frac{L_S}{2} - aL_S \right] \cap \left[\frac{L_S}{2} + aL_S, L_S \right] \end{cases} . \quad \text{(S31)}$$

The profile of the thickness is shown in Fig. S4e. For the target surfaces with other types of generatrix, the inner ribbons are needed in the 2D precursors as illustrated in Fig. 3(A and B). Moreover, setting the middle part as the bonding site introduces more feasible target surfaces for the inverse design, as presented in Fig.3(C and D) with similar design strategy shown in Fig.S4.

S2.2 Examples

We start from the structures in Fig. 2b.

A (Hemisphere)

The coordinates of the generatrix are

$$\begin{cases} X(S) = -R\cos\dfrac{S}{R} \\ Z(S) = R\sin\dfrac{S}{R} \end{cases}, S \in [0, L_S], \quad \text{(S32)}$$

in which the radius $R = 14\ \text{mm}$, and the arc length $L_S = \pi R$. Substitution of Eq. (S32) into Eqs. (S30) and (S31) gives

$$w(S) = \frac{2\pi R}{n}\left|\cos\frac{S}{R}\right|,\ S \in \left[0, \frac{L_S}{2} - aL_S\right] \cap \left[\frac{L_S}{2} + aL_S, L_S\right], \tag{S33}$$

$$t(S) = \begin{cases} t_{\max},\ S \in \left(\dfrac{L_S}{2} - aL_S, \dfrac{L_S}{2} + aL_S\right) \\ t_{\max}\left(\left|\tan(a\pi)\tan\dfrac{S}{R}\right|\right)^{\frac{1}{3}},\ S \in \left[0, \dfrac{L_S}{2} - aL_S\right] \cap \left[\dfrac{L_S}{2} + aL_S, L_S\right] \end{cases}, \tag{S34}$$

where the small parameter $a = 0.05$, the number $n = 10$, and the maximum thickness $t_{\max} = 0.512\ \text{mm}$.

B (Drum)

The coordinates of the generatrix is a piecewise function

$$\begin{aligned} X(r) &= \begin{cases} -21 + 5\cos\dfrac{\pi}{8} - 5\cos\left(\dfrac{1+r}{4}\pi\right),\ -1 \le r < -\dfrac{1}{2} \\ 21\sin(\pi r),\ -\dfrac{1}{2} \le r \le \dfrac{1}{2} \\ 21 - 5\cos\dfrac{\pi}{8} + 5\cos\left(\dfrac{1-r}{4}\pi\right),\ \dfrac{1}{2} \le r \le 1 \end{cases} \\ Z(r) &= \begin{cases} 21\sin\left(\dfrac{1+r}{4}\pi\right),\ -1 \le r < -\dfrac{1}{2} \\ 5\cos(\pi r) + 21\sin\dfrac{\pi}{8},\ -\dfrac{1}{2} \le r \le \dfrac{1}{2} \\ 21\sin\left(\dfrac{1-r}{4}\pi\right),\ \dfrac{1}{2} \le r \le 1 \end{cases} \end{aligned} \tag{S35}$$

and the arc length and the arc coordinate are given by

$$\begin{aligned} L_S &= \int_{-1}^{1}\sqrt{\left(\frac{\mathrm{d}Z(\xi)}{\mathrm{d}\xi}\right)^2 + \left(\frac{\mathrm{d}X(\xi)}{\mathrm{d}\xi}\right)^2}\,\mathrm{d}\xi \\ S &= \int_{-1}^{r}\sqrt{\left(\frac{\mathrm{d}Z(\xi)}{\mathrm{d}\xi}\right)^2 + \left(\frac{\mathrm{d}X(\xi)}{\mathrm{d}\xi}\right)^2}\,\mathrm{d}\xi \end{aligned}. \tag{S36}$$

The curvature of the generatrix is positive everywhere and meets the condition in Eq. (S8). The width $w(S)$ and the thickness $t(S)$ of the 2D precursor are obtained from Eqs. (S30) and (S31). The maximum thickness is set as $t_{\max} = 0.512\ \text{mm}$.

C (Fire ballon)

The coordinates of the generatrix are

$$\begin{cases} X(r) = 20\sin r + 20\sin(4r) \\ Z(r) = 60\cos r + 30\cos(2r) - 60\cos(0.772) - 30\cos(1.544) \end{cases}, r \in [-0.772, 0.772] \quad \text{(S37)}$$

and the arc length and the arc coordinate are given by

$$\begin{aligned} L_S &= \int_{-0.772}^{0.772} \sqrt{\left(\frac{\mathrm{d}Z(\xi)}{\mathrm{d}\xi}\right)^2 + \left(\frac{\mathrm{d}X(\xi)}{\mathrm{d}\xi}\right)^2}\,\mathrm{d}\xi \\ S &= \int_{-0.772}^{r} \sqrt{\left(\frac{\mathrm{d}Z(\xi)}{\mathrm{d}\xi}\right)^2 + \left(\frac{\mathrm{d}X(\xi)}{\mathrm{d}\xi}\right)^2}\,\mathrm{d}\xi \end{aligned} . \quad \text{(S38)}$$

The curvature of the generatrix is positive everywhere, and the width $w(S)$ and the thickness $t(S)$ of the 2D precursor are obtained from Eqs. (S30) and (S31) with the maximum thickness $t_{\max} = 0.608\ \text{mm}$.

Next, we move on to the microscale structures illustrated in Fig. 2c.

A (Microscale experiment (Hemisphere))

The coordinate function of the generatrix is the same as Eq. (S32) with the radius $R = 2\ \text{mm}$. The width and the theoretical thickness are derived from Eqs. (S33) and (S34) with the maximum thickness $t_{\max} = 10\ \mu\text{m}$. The thickness

distribution designed for the microscale experiment is obtained by discretizing $t(S)$ using Eq. (S28).

B (Microscale experiment (Drum))

The generatrix shape is one tenth of the macroscale structure illustrated in Fig. 2b.

$$\begin{cases} X(r)=\begin{cases} -\frac{21}{10}+\frac{1}{2}\cos\frac{\pi}{8}-\frac{1}{2}\cos\left(\frac{1+r}{4}\pi\right), & -1\le r<-\frac{1}{2} \\ \frac{21}{10}\sin(\pi r), & -\frac{1}{2}\le r\le\frac{1}{2} \\ \frac{21}{10}-\frac{1}{2}\cos\frac{\pi}{8}+\frac{1}{2}\cos\left(\frac{1-r}{4}\pi\right), & \frac{1}{2}\le r\le 1 \end{cases} \\ Z(r)=\begin{cases} \frac{21}{10}\sin\left(\frac{1+r}{4}\pi\right), & -1\le r<-\frac{1}{2} \\ \frac{1}{2}\cos(\pi r)+\frac{21}{10}\sin\frac{\pi}{8}, & -\frac{1}{2}\le r\le\frac{1}{2} \\ \frac{21}{10}\sin\left(\frac{1-r}{4}\pi\right), & \frac{1}{2}\le r\le 1 \end{cases} \end{cases}. \tag{S39}$$

The maximum thickness is set as $t_{\max}=10\,\mu\text{m}$, and the resulting thickness distribution is shown in Fig. 2c.

In Fig. 3, the geometrical information of other target surfaces is presented below

A (Donut)

The generatrix coordinates are given as

$$\begin{cases} Z(S)=\frac{1}{90}\left[L_S-L_S\cos\frac{2\pi S}{L_S}-9\pi\left(S-\frac{L_S}{2}\right)\sin\frac{2\pi S}{L_S}\right] \\ X(S)=\int_0^S\left[1-\left(\frac{\mathrm{d}Z(\xi)}{\mathrm{d}\xi}\right)^2\right]^{\frac{1}{2}}\mathrm{d}\xi \end{cases}, S\in[0,L_S], \tag{S40}$$

in which the arc length $L_S = 50\,\text{mm}$. The curvature of the generatrix has two zero points, and thus at least one vertical concentrated force G should be applied to the ribbon. Due to the symmetry of the generatrix shape, the location of the vertical concentrated force G is in the middle of the ribbon ($S = L_S/2$). In experiment, we set an inner ribbon at each joint of the middle part and the ribbon part, and the inner ribbon provides the concentrated force with magnitude $G/2$ in the deformed configuration. The arc length, the bonding length, the width and the thickness of the inner ribbon are L_{ribbon}=1.8563 mm , $L_{\text{ribbon-bonding}} = 2.0840\ \text{mm}$, $w_{\text{ribbon}} = 0.52101\,\text{mm}$ and $t_{\text{ribbon}} = 0.096\,\text{mm}$, respectively. The bonding length and the maximum thickness of the large ribbon are $L_{\text{bonding}} = 18.770\,\text{mm}$ and $t_{\max} = 0.512\,\text{mm}$. The width of the large ribbon can be obtained from Eq. (S30). The pre-strain of the substrate is $\varepsilon_{\text{pre}} = 0.086503$. The detailed approach for the thickness distribution of the large ribbon is given in **Sec. S1.1**.

B (Complex surface)

The coordinates of the generatrix are

$$\begin{cases} Z(S) = \dfrac{L_S}{120}\left[5 - 5\sqrt{5} + 16\cos\left(\dfrac{4\pi S}{5L_S} - \dfrac{2\pi}{5}\right) + 4\cos\left(\dfrac{24\pi S}{5L_S} - \dfrac{2\pi}{5}\right)\right] \\ X(S) = \displaystyle\int_0^S \left[1 - \left(\frac{\mathrm{d}Z(\xi)}{\mathrm{d}\xi}\right)^2\right]^{\frac{1}{2}} \mathrm{d}\xi \end{cases}, S \in [0, L_S], \qquad \text{(S41)}$$

in which the arc length $L_S = 120\,\text{mm}$. The curvature of the generatrix has four zero points, and at least two vertical concentrated forces are needed to apply to

the ribbon to satisfy the static equilibrium condition. The locations of these two forces are $S_1 = 39.492$ and $S_2 = 80.508$. The arc length, the bonding length, the width and the thickness of the inner ribbon are L_{ribbon}=21.109 mm , $L_{\text{ribbon-bonding}}$=3.7993 mm , $w_{\text{ribbon}} = 3.7993$ mm and $t_{\text{ribbon}} = 0.096$ mm , respectively. The bonding length and the maximum thickness of the large ribbon are $L_{\text{bonding}} = 22.962$ mm and $t_{\max} = 0.32$ mm . The width of the large ribbon can be obtained from Eq. (S30). The pre-strain of the substrate is $\varepsilon_{\text{pre}} = 0.076213$. The detailed approach for the thickness distribution of the large ribbon is given in **Sec. S1.1**.

C (Flower)

The middle part of the surface is designed as the bonding site. The axis shape of the ribbon is composed of two arcs, defined by

$$\begin{cases} Z(S) = \begin{cases} R\left[\cos\left(\dfrac{S}{R} - \dfrac{\alpha}{2}\right) - \cos\dfrac{\alpha}{2}\right], S \in [0, \alpha R] \\ R\left[\cos\left(\dfrac{S}{R} - \dfrac{3\alpha}{2}\right) - \cos\dfrac{\alpha}{2}\right], S \in [\alpha R, 2\alpha R] \end{cases} \\ X(S) = \begin{cases} -\dfrac{25}{2\pi} + R\left[\sin\left(\dfrac{S}{R} - \dfrac{\alpha}{2}\right) - \sin\dfrac{\alpha}{2}\right], S \in [0, \alpha R] \\ \dfrac{25}{2\pi} + R\left[\sin\left(\dfrac{S}{R} - \dfrac{3\alpha}{2}\right) + \sin\dfrac{\alpha}{2}\right], S \in [\alpha R, 2\alpha R] \end{cases} \end{cases}, \tag{S42}$$

in which the radius $R = 60/\pi$ mm and the central angle $\alpha = 5\pi/6$. The width distribution $w(S)$ of the half ($S \in [0, \alpha R/2] \cap [\alpha R, 3\alpha R/2]$) near the middle bonding is obtained from Eq. (S30) for the centrally symmetric surface. The width of the other half ($S \in [\alpha R/2, \alpha R] \cap [3\alpha R/2, 2\alpha R]$), which is treated as supporting part, is

set as constant $w = 5\,\text{mm}$. The thickness distribution $t(S)$ can be obtained from Eq. (S6) with the maximum thickness $t_{\max} = 0.32\,\text{mm}$.

D (Concave lens (270°))

The generatrix shape consists of three arcs. The radii and the central angles of the left, middle and right arcs are $(R, \alpha) = \left(60\,\text{mm}, 2\text{arc}\csc\left(4\sqrt{\left(3-2\sqrt{2}\right)\left(5-\sqrt{5}\right)}\right)\right)$, $(15\,\text{mm}, 3\pi/2)$ and $\left(60\,\text{mm}, 2\text{arc}\csc\left(4\sqrt{\left(3-2\sqrt{2}\right)\left(5-\sqrt{5}\right)}\right)\right)$ respectively. We model the half of the generatrix as the combined ribbon model presented in **Sec. S1.2**. Similar to the structure C, the widths of middle ribbon parts ($R = 15\,\text{mm}$) are obtained from Eq. (S30) serving as components of the concave lens, while the widths of the ribbon parts with radius $R = 60\,\text{mm}$ are set as constant $w = 3\sqrt{2}\pi/2\,\text{mm}$ to serve as supporting ribbons. Besides, we design the small middle part as bonding site in the 2D precursor. The inverse design approach of the ribbons is the same as the combined ribbons in **Sec. S1.2**.

Below are the structures demonstrated in Fig. S5

A (Ellipsoidal surface)

The coordinates of the generatrix are given as

$$\begin{cases} Z = 7\cos(\pi r) \\ X = 21\sin(\pi r) \end{cases}, r \in \left[-\frac{1}{2}, \frac{1}{2}\right] \tag{S43}$$

and the arc length and the arc coordinate are given by

$$\begin{aligned} L_S &= \int_{-\frac{1}{2}}^{\frac{1}{2}} \sqrt{\left(\frac{\mathrm{d}Z(\xi)}{\mathrm{d}\xi}\right)^2 + \left(\frac{\mathrm{d}X(\xi)}{\mathrm{d}\xi}\right)^2}\,\mathrm{d}\xi \\ S &= \int_{-\frac{1}{2}}^{r} \sqrt{\left(\frac{\mathrm{d}Z(\xi)}{\mathrm{d}\xi}\right)^2 + \left(\frac{\mathrm{d}X(\xi)}{\mathrm{d}\xi}\right)^2}\,\mathrm{d}\xi \end{aligned} . \tag{S44}$$

Since the generatrix curvature $K(S)$ is positive everywhere, the width $w(S)$ and the thickness $t(S)$ are obtained using Eqs. (S30) and (S31).

B (Concave lens (180°)) and C (Concave lens (120°))

The inverse design approaches of structure B and C are the same as the structure D (concave lens (270°)) in Fig. 3. Here we only give the geometric parameters of the generatrices of structure B and C. The generatrix shape is also made up of three arcs. In structure B, the radii and the central angles of the left, middle and right arcs are $(R,\alpha)=\left(60\ \mathrm{mm}, 2\mathrm{arc}\csc\left(2\sqrt{10-2\sqrt{5}}\right)\right)$, $(15\ \mathrm{mm}, \pi)$ and $\left(60\ \mathrm{mm}, 2\mathrm{arc}\csc\left(2\sqrt{10-2\sqrt{5}}\right)\right)$, respectively. In structure C, the radii and the central angles of the left, middle and right arcs are $(R,\alpha)=(30\ \mathrm{mm}, \pi/3)$, $(30\ \mathrm{mm}, 2\pi/3)$ and $(30\ \mathrm{mm}, \pi/3)$, respectively.

S3 Inverse design of general 3D surfaces

S3.1 Inverse design approach

As illustrated in Fig. S6, we obtain several (n) curves of the cross sections by CT scanning the general surface along the Y axis, without loss of generality, and then exploit the curvy ribbons with the same shapes to reconstruct the

surface. The largest vertical distance between the adjacent ribbons denote the error of this approximation approach, i.e.,

$$\delta = \max\left[\left|Z\left(X,Y_{(i)}\right)-Z\left(X,Y_{(i+1)}\right)\right|\right], i \in \{1,2,\cdots,n-1\}, \tag{S45}$$

in which n is the scanning number, and $Z(X,Y)$ is the target surface function, and $Z\left(X,Y_{(i)}\right)$ is the curve function of the ribbon with location $Y_{(i)}$

$$Y_{(i)}=Y_{\min}+\left(i-\frac{1}{2}\right)\frac{Y_{\max}-Y_{\min}}{n}, \tag{S46}$$

in which $Y_{\min}$ and $Y_{\max}$ are the maximum and minimum values of coordinate Y of the target surface. The range of coordinate X in Eq. (S45) is defined as

$$X \in \left[\max\left(X_{\min(i)},X_{\min(i+1)}\right),\min\left(X_{\max(i)},X_{\max(i+1)}\right)\right], \tag{S47}$$

in which $X_{\min(i)}=\min\left\{\text{root}\left[Z\left(X,Y_{(i)}\right)=0\right]\right\}$ and $X_{\max(i)}=\max\left\{\text{root}\left[Z\left(X,Y_{(i)}\right)=0\right]\right\}$ are the X coordinates of the ribbon ends. The error δ (Eq. (S45)) decreases with the scanning number n for a given surface $Z(X,Y)$. The width of each ribbon can be written as

$$w=\frac{\left(Y_{\max}-Y_{\min}\right)}{n}. \tag{S48}$$

Then the inverse design of the general surface is converted into the inverse design of curvy ribbons presented in **Sec. S1**. Below we give the inverse design details of the target general surfaces studied in this paper.

S3.2 Examples

Figure. 4b illustrates two general surfaces.

A (Saddle)

The saddle surface function is

$$Z(X,Y)=20-\frac{X^2}{40}+\frac{Y^2}{70},\ Y\in[Y_{\min},Y_{\max}]=[-30,30],\ Z\geq 0\,. \tag{S49}$$

Substitution of Eq. (S49) into Eq. (S46) gives the location $Y_{(i)}$

$$Y_{(i)}=-32+4i,\ i=1,2,3,\cdots n\,. \tag{S50}$$

Thus the axis curve functions of the ribbons are

$$Z_{(i)}(X)=Z\left(X,Y_{(i)}\right)=20-\frac{X^2}{40}+\frac{Y_{(i)}^2}{70},\ i=1,2,3,\cdots n\,. \tag{S51}$$

The range of coordinate X is

$$X\in\left[X_{\min(i)},X_{\max(i)}\right]=\left[-2\sqrt{200+\frac{Y_{(i)}^2}{7}},2\sqrt{200+\frac{Y_{(i)}^2}{7}}\right]. \tag{S52}$$

and the arc length and the arc coordinate are given by

$$\begin{aligned}L_{S(i)}&=\int_{-2\sqrt{200+\frac{Y_{(i)}^2}{7}}}^{2\sqrt{200+\frac{Y_{(i)}^2}{7}}}\sqrt{1+\left(\frac{\mathrm{d}Z_{(i)}(\xi)}{\mathrm{d}\xi}\right)^2}\,\mathrm{d}\xi\\ S&=\int_{-2\sqrt{200+\frac{Y_{(i)}^2}{7}}}^{X}\sqrt{1+\left(\frac{\mathrm{d}Z_{(i)}(\xi)}{\mathrm{d}\xi}\right)^2}\,\mathrm{d}\xi\end{aligned}\,. \tag{S53}$$

The bonding lengths of the ribbons is given as

$$L_{\text{bonding}(i)}=\frac{\left[L_{S(i)}-\left(X_{(i)\max}-X_{(i)\min}\right)\right]\left(\varepsilon_{\text{pre}}+1\right)}{\varepsilon_{\text{pre}}}-L_{S(i)},\ i=1,2,3,\cdots n\,, \tag{S54}$$

in which ε_{pre} is the pre-strain of the substrate. In FEA and experiment, we set the scanning number as $n=15$ and the pre-strain as $\varepsilon_{\text{pre}}=0.17586$. The curvatures

of those ribbons are positive, and hence the thickness distribution can be obtained using Eq. (S6) with the width $w = 4\,\text{mm}$ (Eq. (S48)) and the maximum thickness $t_{\max} = 0.32\,\text{mm}$.

B (Waterdrop)

The surface function is given by

$$\begin{cases} X = 30\sin r \sin\dfrac{r}{2}\cos\theta \\ Y = 30\cos r \\ Z = 30\sin r \sin\dfrac{r}{2}\sin\theta \end{cases}, r \in [0,\pi], \theta \in [0,\pi], \tag{S55}$$

from which we obtain $Y_{\max} = 30$ and $Y_{\min} = -30$. Then the location $Y_{(i)}$ (Eq. (S46)) can be written as

$$Y_{(i)} = -30 + \frac{(60i - 30)}{n}. \tag{S56}$$

Combining Eqs. (S55) and (S56), we obtain the axis coordinates of the ribbons

$$\begin{cases} X_{(i)} = 30\sin\left(\arccos\left(-1 + \dfrac{(2i-1)}{n}\right)\right)\sin\dfrac{\arccos\left(-1 + \dfrac{(2i-1)}{n}\right)}{2}\cos\theta \\ Z_{(i)} = 30\sin\left(\arccos\left(-1 + \dfrac{(2i-1)}{n}\right)\right)\sin\dfrac{\left(\arccos\left(-1 + \dfrac{(2i-1)}{n}\right)\right)}{2}\sin\theta \end{cases}, \theta \in [0,\pi]. \tag{S57}$$

In the FEA and the experiment, we set the scanning number as $n = 15$. Since the shape of the ribbon of $i = 15$ is too small, we take the ribbons of $i = 1 \sim 14$ to reconstruct the target surface. The bonding length $L_{\text{bonding}(i)}$ is obtained from Eq. (S54) with the pre-strain $\varepsilon_{\text{pre}} = 0.42239$. The ribbons' semicircle axial shapes

allow us to determine their thickness distribution from Eq. (S22) with the central angle $\alpha = \pi$, the width $w = 4\,\text{mm}$ and the maximum thickness $t_{\max} = 0.32\,\text{mm}$.

In Fig. 4c and Fig. S7, we demonstrate the inverse design results of a rodent model[1]. We use commercial software SIMPLIFY3D to divide the 3D model into 70 segments. The edge data of these segments are detected by edge detection function in MATLAB. Then, we use ellipse curves to fit these edges and obtain the geometrical data of the ellipse curves in MATLAB environment. Finally, the curvy ribbons are designed to meet the shape of the ellipse curves based on the inverse design solutions in **Sec. S1**. Different from the above structures, the bonding thickness of each ribbon of rodent model is regarded as a design parameter for the inverse design of the suspended ribbons, and is illustrated in the bar chart in Fig. S7b.

S4 Cartoon face

In Fig. S8, we illustrated the inverse design of a cartoon face with spherical eyes and conical nose and lip. The surface functions are given by

$$\begin{cases} X_{\text{left-eye}}(r,\theta) = -25 + 10\sqrt{2}\left(-1+\sqrt{3}\right)\cos\theta\sin\left(\dfrac{1}{20}\sqrt{2+\sqrt{3}}r\right) \\ Y_{\text{left-eye}}(r,\theta) = 10\sqrt{2}\left(-1+\sqrt{3}\right)\sin\theta\sin\left(\dfrac{1}{20}\sqrt{2+\sqrt{3}}r\right) \\ Z_{\text{left-eye}}(r,\theta) = 5\left(1-\sqrt{3}\right)\left[-1+\sqrt{3}-2\sqrt{2}\cos\left(\dfrac{1}{20}\sqrt{2+\sqrt{3}}r\right)\right] \end{cases} \tag{S58}$$

[1] https://free3d.com/3d-model/low-poly-rat-3205.html

$$\begin{cases} X_{\text{right-eye}}(r,\theta) = 25 + 10\sqrt{2}\left(-1+\sqrt{3}\right)\cos\theta\sin\left(\dfrac{1}{20}\sqrt{2+\sqrt{3}}r\right) \\ Y_{\text{right-eye}}(r,\theta) = 10\sqrt{2}\left(-1+\sqrt{3}\right)\sin\left(\dfrac{1}{20}\sqrt{2+\sqrt{3}}r\right)\sin\theta \\ Z_{\text{right-eye}}(r,\theta) = 5\left(1-\sqrt{3}\right)\left[-1+\sqrt{3}-2\sqrt{2}\cos\left(\dfrac{1}{20}\sqrt{2+\sqrt{3}}r\right)\right] \end{cases} \tag{S59}$$

$$\begin{cases} X_{\text{nose}}(r,\theta) = -\dfrac{\left(25\pi+3\sqrt{2+\sqrt{3}}r\right)\cos\dfrac{\theta}{2}}{5\pi} \\ Y_{\text{nose}}(r,\theta) = -20-\dfrac{12\sqrt{2+\sqrt{3}}r}{5\pi} \\ Z_{\text{nose}}(r,\theta) = \dfrac{3\left(25\pi+3\sqrt{2+\sqrt{3}}r\right)\sin\dfrac{\theta}{2}}{20\pi} \end{cases} \tag{S60}$$

$$\begin{cases} X_{\text{mouth-left}}(r,\theta) = -10+\dfrac{6\sqrt{2+\sqrt{3}}r}{5\pi} \\ Y_{\text{mouth-left}}(r,\theta) = -55-\left(\dfrac{5}{2}+\dfrac{3\sqrt{2+\sqrt{3}}r}{10\pi}\right)\cos\dfrac{\theta}{2} \\ Z_{\text{mouth-left}}(r,\theta) = \dfrac{\left(75\pi+9\sqrt{2+\sqrt{3}}r\right)\sin\dfrac{\theta}{2}}{40\pi} \end{cases}$$

$$\begin{cases} X_{\text{mouth-right}}(r,\theta) = 10-\dfrac{6\sqrt{2+\sqrt{3}}r}{5\pi} \\ Y_{\text{mouth-right}}(r,\theta) = -55-\left(\dfrac{5}{2}+\dfrac{3\sqrt{2+\sqrt{3}}r}{10\pi}\right)\cos\dfrac{\theta}{2} \\ Z_{\text{mouth-right}}(r,\theta) = \dfrac{\left(75\pi+9\sqrt{2+\sqrt{3}}r\right)\sin\dfrac{\theta}{2}}{40\pi} \end{cases} \tag{S61}$$

in which

$$r \in \left[-\frac{25}{3}\sqrt{2-\sqrt{3}}\pi, \frac{25}{3}\sqrt{2-\sqrt{3}}\pi\right], \theta \in [0, 2\pi] \tag{S62}$$

The eyes and the nose are treated as the centrally symmetric surfaces and the general surface, respectively. The corresponding inverse design strategies in

Sec. S2 and **S3** are adopted to generate the 2D precursor. For experimental convenience, we utilize three membranes to reconstruct the mouth and the upper part of the nose, as illustrated in 2D precursor. The FEA and experimental results are in a good agreement with the target structure.

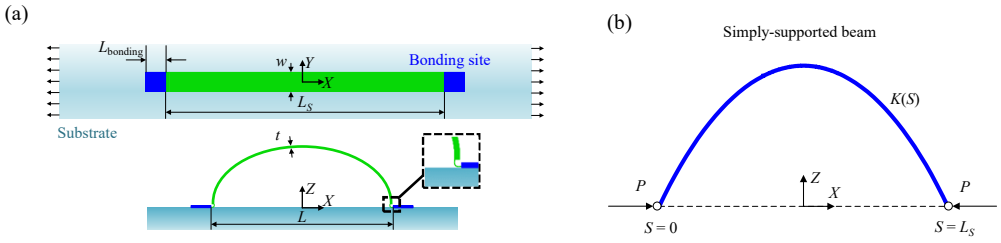

Figure S1. A simply-supported ribbon subjected to uniaxial forces. (a) Schematic of mechanically guided 3D assembly for a curvy ribbon with creases in the ends. (b) Illustration of a mechanics model for the simply-supported ribbon.

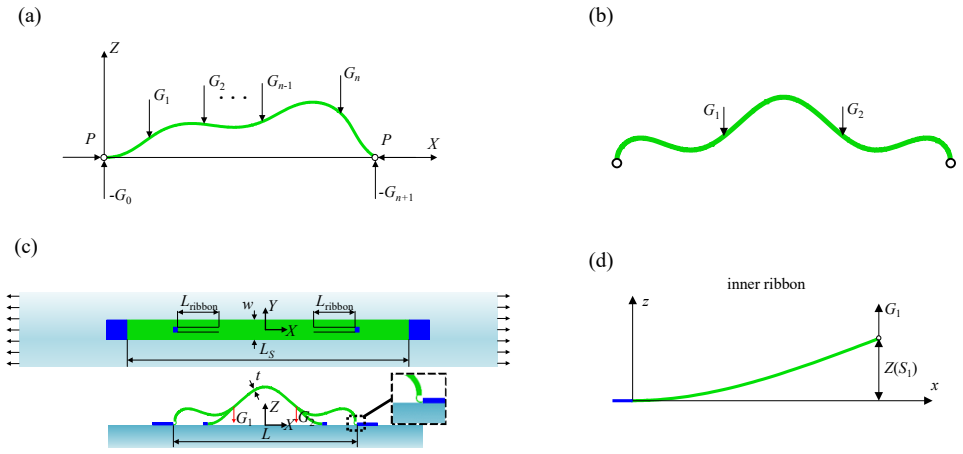

Figure S2. A simply-supported ribbon subjected to uniaxial and vertical forces. (a) Free-body diagram of a simply-supported ribbon subjected to the vertical concentrated forces. (b) A symmetric, simply-supported ribbon subjected to the forces G_1 and G_2. (c) Schematic of mechanically guided 3D assembly for the target ribbon with two inner ribbons designed in the 2D precursor. (d) A cantilever ribbon model for the small inner ribbon.

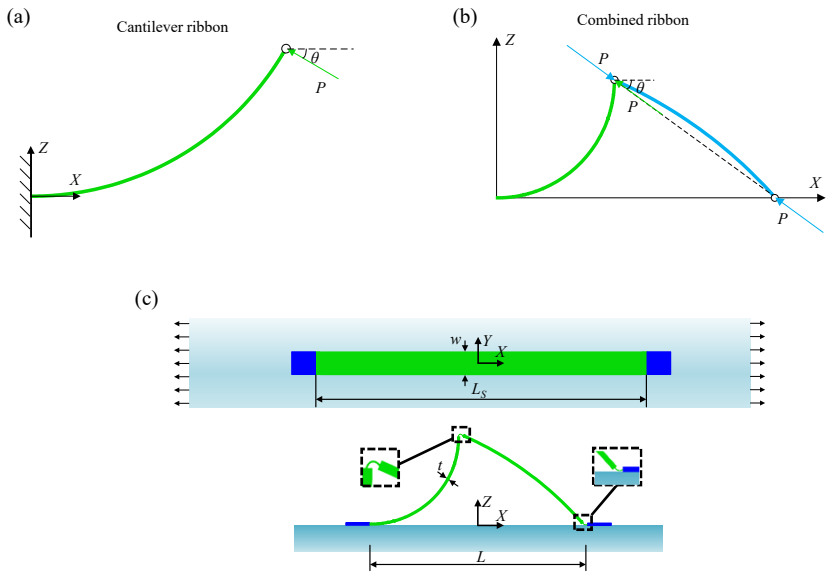

Figure S3. Combined ribbon. (a) Mechanical model for cantilever ribbon. (b) Mechanical model for combined ribbon. (c) Schematic of mechanically 3D assembly for the combined ribbon.

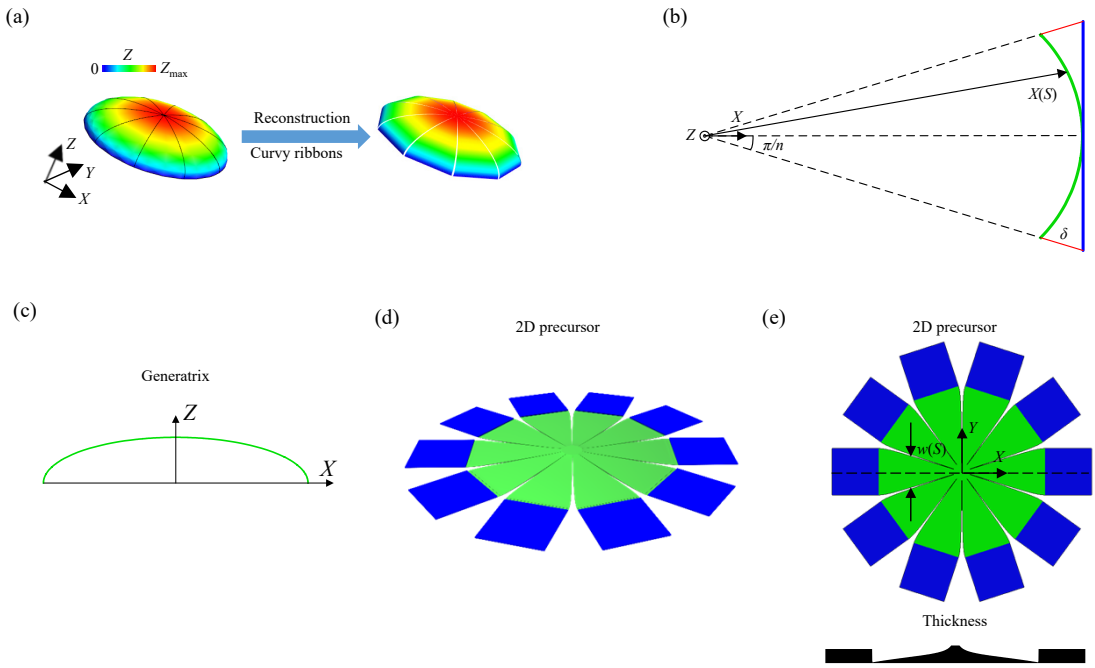

Figure S4. Inverse design for centrally symmetric surfaces. (a) Approximation approach for centrally symmetrical surfaces. (b) Schematic of the error induced by the approximation. (c) The generatrix of the target surface. (d) The 2D precursor from a 3D view. (e) The 2D precursor from the top view and the profile of the thickness distribution.

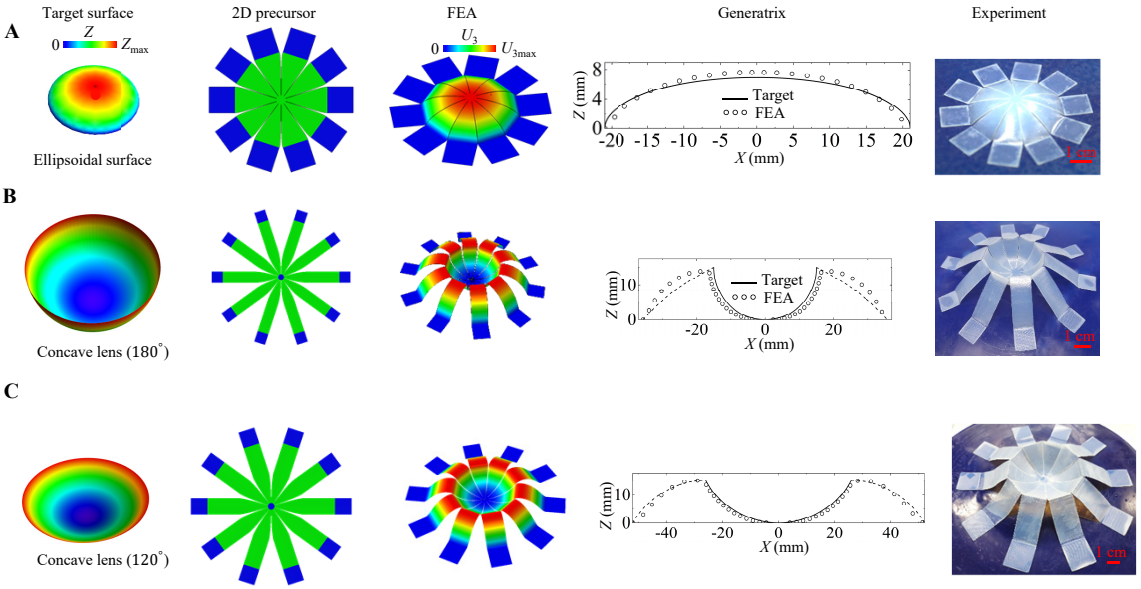

Figure S5. 2D precursors, optical images and FEA results for the ellipsoidal surface (A), concave lens (180°) (B) and concave lens (120°) (C).

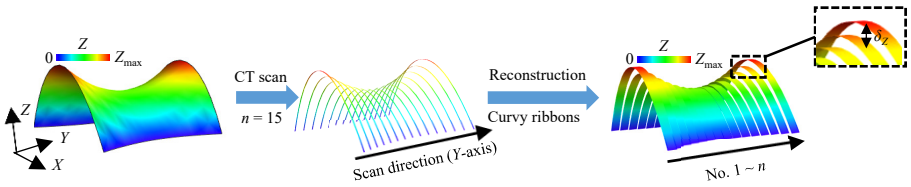

Figure S6. Approximation approach for the general surface based on the CT-inspired discretization.

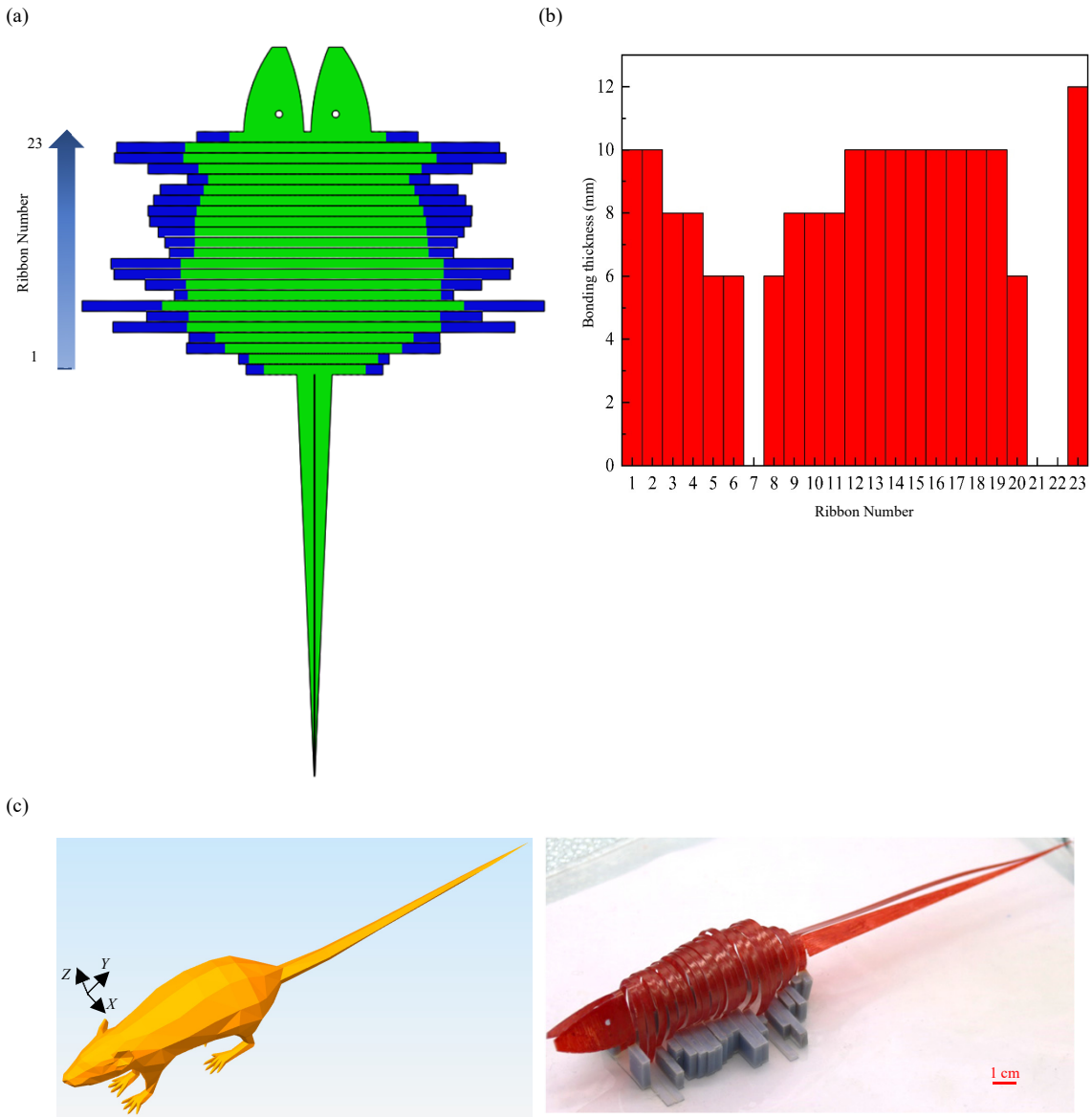

Figure S7. 2D precursors (a), the height distribution of bonding sites (b) and 3D structure based on centimeter-scale experiment (c) for the rodent model in Figure 4c.

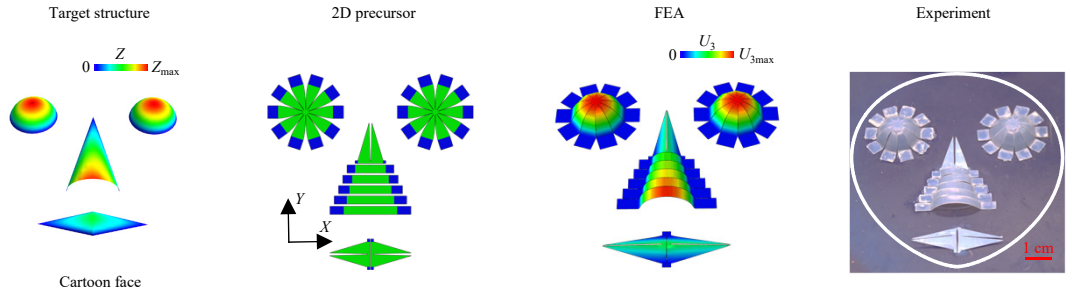

Figure S8. Results of the inverse design for a cartoon face, including the 2D precursor, optical image and FEA calculations.